Proceedings of the Combustion Institute 40 (2024) 105430

Contents lists available at ScienceDirect

Proceedings of the Combustion Institute

journal homepage: www.elsevier.com/locate/proci

Mitigating thermoacoustic instabilities in premixed hydrogen flames using axial staging

Aksel Ånestad *, Eirik Æsøy, James R. Dawson, Nicholas A. Worth

Norwegian University of Science and Technology, Trondheim, Norway

ARTICLE INFO

Keywords:
Combustion instabilities
Sequential combustion
Hydrogen
Axial staging

ABSTRACT

In this paper we demonstrate how axial staging can be utilised to mitigate thermoacoustic instabilities in a combustion system by flame redistribution. This is achieved by moving flow to a second stage flame while keeping the combined thermal power and total flow fixed. The stability of the system was first characterised for premixed H_2-CH_4-air flames operated with hydrogen volume fraction in the range 80%–100%. As observed in recent work, increasing the hydrogen concentration led to the onset of strong self-excited instabilities. Increasing the flow velocity for a fixed hydrogen concentration was shown to have the same effect. Both of these are linked to a decrease in the convective time scale — causing the flame to become more convectively compact and responsive to higher frequencies. We then show that these instabilities could be reduced for all conditions, by distributing flow to the secondary flame. Two main driving mechanisms causing suppression were observed and analysed. Firstly, a reduction in the flow rate provided to the first stage flame, leading to a corresponding change in the flame structure. This leads to an increase in the convective time scale. This effect is quantified by a reduced gain at higher frequencies, and a change in the time delay of the flame transfer function. Secondly, introducing a second flame with a different convective time scale results in interference between the two flames. This acts to suppress or enhance the global fluctuations in heat release rate and hence, the amplitude of the pressure oscillations in the system.

1. Introduction

Gas turbines are a key element of the current worldwide energy production infrastructure, offering a flexible and efficient way to produce power on demand. However, while natural gas turbines offer a reduction in emissions relative to oil and coal, they still produce a significant amount of CO_2. One way to eliminate these emissions is through the use of carbon-free fuels, such as hydrogen [1,2] and ammonia [3–5]. As a result of their vastly different chemical properties compared to those of methane, this transition poses a range of technical challenges. Combined with the need to balance out the variability of renewable energy sources, and limited availability of carbon-free fuels at scale, this creates a need for load-flexible systems capable of burning both conventional and novel fuels. Additionally, a major issue connected to hydrogen combustion is the occurrence of potentially damaging thermoacoustic instabilities [1,2,6–15].

Self-excited thermoacoustic instabilities occur when there is a coupling between the heat release rate (HRR) from the flame and the acoustic mode(s) of the combustor geometry [6,16,17]. Several recent studies have investigated the effect of hydrogen-enriched methane [7,9,11] and pure hydrogen [10–14,18] on the combustion dynamics. A series of studies [10–12,18] used various multiple injector geometries to study premixed pure hydrogen combustion dynamics. Lee and Kim [12], and Kang and Kim [10,11] showed how hydrogen flames in a multi nozzle array consistently excites higher longitudinal eigenmodes (up to 1.8 kHz). Similarly, Lee and Kim [18] recorded transverse and spinning instabilities in excess of 3.4 kHz with a multi-slit flame array. Work on premixed H_2-CH_4-air flames by Æsøy et al. [9,19,20], show that increasing H_2 significantly shortens the flame and therefore the convective time delay. This results in Flame Transfer Functions (FTFs) with wider bandpass characteristics, meaning significant gain at much higher frequencies.

Sequential combustion systems have recently gained interest due to their inherent operational and fuel flexibility [1,3,5,21,22]. As a result, several recent studies have reported unique thermoacoustic interactions between axially staged flames [13–15,23–25]. Experiments by Choi and Kim [13] used a premixed sequential combustor to show the importance of the second-stage flame's position relative to the acoustic mode-shape, demonstrating that despite identical nozzle geometry, the second-stage flame dynamics preferentially coupled to a

* Corresponding author.
E-mail address: aksel.anestad@ntnu.no (A. Ånestad).

https://doi.org/10.1016/j.proci.2024.105430
Received 4 December 2023; Accepted 13 June 2024
Available online 29 June 2024

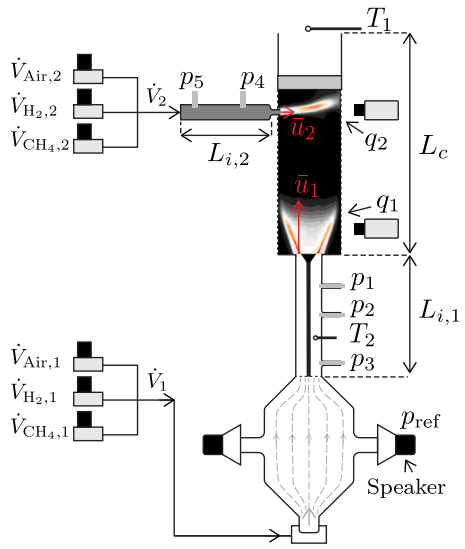

Fig. 1. Schematic of experimental setup and available diagnostics. Alicat MFCs were used to distribute the flow $\dot{V}_1$ and $\dot{V}_2$ between two stages. For more details see [15,29].

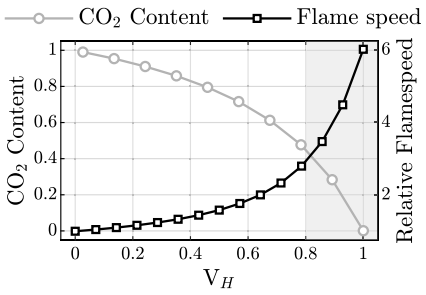

Fig. 2. Carbon content of exhaust gas and relative flame speed vs hydrogen concentration for H_2/CH_4 blends.

higher frequency mode. A series of studies [24–26] have investigated thermoacoustic instabilities in a pressurised reheat combustor. This system emulates the architecture employed in industrial sequential gas turbines such as the Ansaldo GT36 [27], consisting of a technically [26] or fully [24,25] premixed first stage flame, followed by a dilution air port and a second stage autoignition-stabilised flame. As detailed by Schulz et al. [24] through experiments and Large Eddy Simulations, the result is a highly complicated thermoacoustic system sensitive to both temperature, and acoustic velocity and pressure oscillations [24,28]. Previous work by Ånestad et al. [15] introduced a simplified axially staged burner, demonstrating its fuel-flexible properties, and the stabilisation of an initially unstable main flame through staging. Due to the resilience of the second-stage opposing jet flames to flashback, this allowed a $> 40\%$ increase in the global equivalence ratio at an even stage–stage air split, with increased second-stage equivalence ratio.

This paper aims to demonstrate how axial staging can be used to effectively mitigate thermoacoustic instabilities for a range of premixed high H_2 flames. We expand on previous work reported in [15], and use a simple bluff body stabilised main flame [9,19,29], and a secondary jet in crossflow flame [30–32]. Compared to studies based on more realistic reheat type combustors [14,24,28], this setup allows for simplified analysis based on well-established methods [9].

The paper is structured as follows: (i) First the stability of the main flame is investigated in isolation over a range of flow rates, H_2-CH_4-air blends, and combustor lengths. (ii) Then, the effect of staging on the stability is investigated by either redistributing flow from the first to the second stage, or by adding flow to the second stage. (iii) Finally, these effects are investigated in detail through measurements of the forced response, before (iv) the main conclusions are given.

2. Experimental methods

2.1. Setup

The burner geometry is illustrated schematically in Fig. 1 and consists of a simple two-stage combustion system. The first stage flame holder geometry is the same as described in [20,29]. It produces a premixed flame (q_1 in Fig. 1) that stabilises in the wake of a 13 mm diameter bluff body. The bluff body is centred in a 19 mm diameter pipe by a 5 mm diameter rod. After the bluff body the flow expands into a 44 mm diameter combustion chamber. The second stage consists of a 5 mm diameter round jet in cross-flow flame, located 100 mm downstream of the bluff body (q_2 in Fig. 1). The nozzle has an area ratio of 4 and is fed by an injector connected to a semi-infinite tube supplying premixed reactants. This configuration is very similar to the one used in [15]. The combustion chamber length L_c was varied to modify the chamber mode and investigate different frequencies. The injector pipe lengths, denoted $L_{i,1} = 175\,\mathrm{mm}$ and $L_{i,2} = 200\,\mathrm{mm}$, were kept fixed. Additionally, a set of Monacor KU-516 Horn drivers was added to the plenum section of the first stage, to enable measurements of the forced flame response in terms of the Flame Transfer Function, following the same method as previous work [9].

2.2. Diagnostics

To quantify stability, the pressure fluctuations p_{1-5} at positions shown in Fig. 1 were measured using Kulite XCS-093-0.35D (range $0 - 35$ kPa) transducers amplified by an FE-579-TA amplifier. Two Hamamatsu H11902-113 PMTs and two intensified Phantom V2012 high-speed cameras, each equipped with Cerco 2178 UV lenses and band-pass filters with spectral range 310 ± 10 nm, were used to measure OH^*-chemiluminescence and the flame response, as in [20,33]. Mean flame images are shown in Fig. 1, where q_1 and q_2 denote flames produced by the first and second stages, respectively. When integrated spatially, these correspond to the global HRR signals Q_1 and Q_2. Time series signals for pressure p_{1-5}, global HRR Q_{1-2}, and the forcing signal p_{ref} were sampled using 24-bit NI 9234 DAQ at a rate of 51.2 kHz. Additionally, the temperatures indicated T_{1-2} in Fig. 1 were acquired at 2 Hz with K-type thermocouples.

2.3. Staging strategy and operating conditions

The main aim of this paper is to demonstrate how a flexible two-stage system can be utilised to suppress thermoacoustic instabilities that arise when operating the first stage with mixtures of CH_4/H_2/Air. As such, six Alicat mass flow controllers (MFCs) were used to control the flow rates denoted $\dot{V}_{\mathrm{air},1}$, $\dot{V}_{\mathrm{H}_2,1}$, $\dot{V}_{\mathrm{CH}_4,1}$ and $\dot{V}_{\mathrm{air},2}$, $\dot{V}_{\mathrm{H}_2,2}$, $\dot{V}_{\mathrm{CH}_4,2}$. The flow was split into two stages, where $\dot{V}_1$ and $\dot{V}_2$ is the total volume flow delivered to each stage, as indicated in Fig. 1.

Mixtures with volume/mole fraction of hydrogen in the range $\dot{V}_{\mathrm{H}_2}/(\dot{V}_{\mathrm{H}_2} + \dot{V}_{\mathrm{CH}_4}) = 0.8$–1, were considered. As shown in Fig. 2, this range is of particular interest since it leads to the largest reduction of CO_2 emissions (about 50%). However, it is also particularly challenging because of large changes to flame properties such as the flame speed that increases exponentially. For simplicity, the same mixture is provided to both stages with an equivalence ratio $\Phi = 0.35$. This has the advantage of keeping the adiabatic flame temperature fixed regardless of the flow split. Moreover, it has been shown that, when operating with H_2/CH_4 mixtures in the lean regime at constant velocity and equivalence ratio, the flow rate and thermal power are kept approximately fixed [34]. There is also only a small difference in the adiabatic flame temperature with $T_a = 1238$ K for $V_H = 0.8$ and

Table 1
Experimental conditions. Maximum volume ratio between the two stages $\dot{V}_2/\dot{V}_1$, velocities at the base of each flame $\bar{u}_1$ and $\bar{u}_2$, V_H is the hydrogen volume/mole fraction, and L_c the combustion chamber length. The equivalence ratio is $\Phi = 0.35$ and T_a is the adiabatic flame temperature.

		$\dot{V}_2/\dot{V}_1$	$\bar{u}_1$ (m/s)	$\bar{u}_2$ (m/s)	V_H	L_c (m)	T_a (K)
Main	$\dot{V}_2 = 0$	0	7.5–30	0	0.8–1	0.15, 0.2, 0.25	1238–1292
Split	$\dot{V}_1 + \dot{V}_2$ = Fixed	0.8, 0.5, 0.3	7.5–30	0–60	1	0.15, 0.2, 0.25	1292
Increase	$\dot{V}_1$ = Fixed	0.73, 0.36 , 0.24	10, 20, 30	0–60	1	0.15, 0.2, 0.25	1292

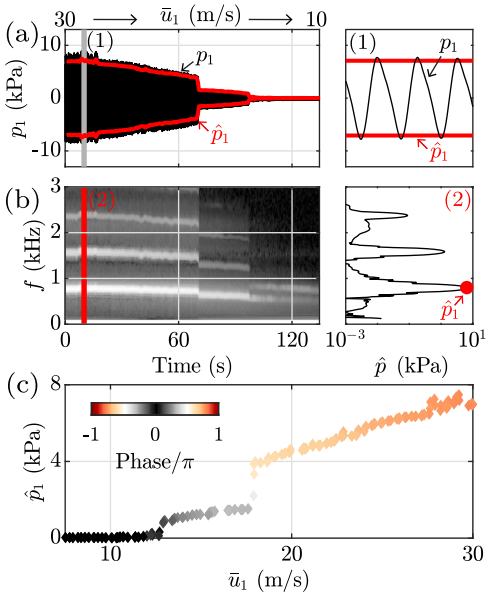

Fig. 3. Time series for $V_H = 1$ and $L_c = 0.2$ m where $\bar{u}_1$ is varied. (a) pressure p_1, (b) spectrogram between p_1 and Q_1, and (c) amplitude of p_1 coloured by the phase difference in between p_1 and Q_1. The red lines in (a) denote the amplitude $\pm\hat{p}_1$ from (b) and panels (1–2) correspond to the grey and red vertical lines at $t = 10$ s.

$T_a = 1292$ K for $V_H = 1$. This is however not a limitation in these systems, where each stage can be fed with different fuel mixtures, as explored in [15]. The volume flows provided to each stage are varied such that the exit velocities were $\bar{u}_1 = 7.5$–32.5 m/s at the bluff body exit of stage 1, and $\bar{u}_2 = 1$–60 m/s at the jet exit of stage 2.

Three staging strategies were investigated. Firstly, the first stage was operated in isolation to establish a reference case with $\dot{V}_2 = 0$. Secondly, the total flow rate was kept fixed but the flow was divided between the two stages; $\dot{V}_1 + \dot{V}_2 =$ Fixed. This implies that a change in the flow rate provided to the second stage results in an inverse change to the flow rate provided to the first stage. Thirdly, the flow rate to the first stage was kept fixed while the flow to the second stage was increased progressively. These cases were selected to investigate whether changes in stability are caused primarily by modifications to the main stage dynamics, interference between the two flames, or a combination of both.

3. Results

3.1. Stability map using main stage

To establish a baseline, the stability of the system is characterised when exclusively operating the first stage, i.e. $\bar{u}_2 = 0$. Values of $\bar{u}_1$, V_H, and L_c were varied systematically as summarised in the first row of Table 1. Fig. 3 shows the effect of slowly varying the velocity in time from $\bar{u}_1 = 30$ to 10 m/s for pure hydrogen ($V_H = 1$) over a period of 120 s. This ramp time was chosen to be sufficiently long to avoid significant hysteresis [35]. In Fig. 3(a) and (b), time series the pressure in the injector pipe p_1, and a corresponding cross-spectrogram between p_1 and Q_1, are shown respectively. The spectrogram is computed using Welch's method and is used to extract the modal amplitude, oscillation frequency, and the phase difference between different signals. In this case, the phase is relative to the global HRR Q_1 measured by the PMT. The red lines in Fig. 3(a) indicate the maximum pressure amplitude $\pm\hat{p}$ for the dominant frequency in (b), and in (c) these are shown against $\bar{u}_1$. When operated at $\bar{u}_1 = 30$ m/s at $t = 0$ s, the system is unstable with a pressure amplitude of about 8 kPa. The pressure amplitude progressively reduces as $\bar{u}_1$ is reduced, and for $\bar{u}_1 < 12$ m/s, the system becomes stable. Note that at $\bar{u}_1 \approx 17$ m/s ($t \approx 70$ s), there is a rapid change in the amplitude, frequency, and phase difference between p_1 and Q_1, indicative of a mode switch.

The same procedure, where the flow rates were varied linearly over 120 s, was repeated for all conditions summarised in the first row of Table 1. The corresponding pressure amplitudes and frequencies are shown in Fig. 4. The first three columns include cases where the hydrogen concentration was varied for $L_c = 0.15$, 0.2, and 0.25 m at fixed values of $\bar{u}_1 = 10$, 20, and 30 m/s. In the fourth column, $\bar{u}_1$ was varied for $V_H = 1$ at different L_c, similar to the data shown in Fig. 3.

A general trend is that the system tends to become unstable for larger values of V_H and $\bar{u}_1$. Furthermore, the frequency increases in jumps at several locations over the same range. This is consistent with previous work on premixed CH_4/H_2 laboratory scale flames [7,8,10–12], where hydrogen tends to trigger instabilities at higher frequencies and amplitudes. As discussed in [7–9] an explanation for this tendency is that an increase in the flame speed leads to a more convectively compact flame. Compactness is quantified by the ratio between the flame length and the flow velocity and can be thought of as a convection time

$$\tau_1 = L_f/\bar{u}_1. \tag{1}$$

It represents the time it takes for convective structures to propagate from the flame base to the flame-front, quantified by the centre of HRR, $L_f = \int \bar{q}_1 x \mathrm{d}x / \int \bar{q}_1 \mathrm{d}x$. The same time scale has also been shown to indicate the gain cut-off frequency [9], which implies that flames with higher hydrogen concentrations or operated at higher velocities can potentially amplify modes at higher frequencies, as discussed by [8].

This is demonstrated in Fig. 5, where the flame structure is shown at different values of V_H and $\bar{u}_1$. The flame length L_f is included as red lines, and τ_1 computed by Eq. (1) are shown in Fig. 5(b). In general, increasing V_H for a fixed $\bar{u}_1$, leads to a shorter flame and hence, a reduction in τ_1. Similarly, τ_1 decreases for an increase in $\bar{u}_1$, although L_f also increases. This occurs because $\bar{u}_1$ increases more rapidly than L_f. Hence, the flame becomes more convectively compact when either $\bar{u}_1$ or V_H is increased. These observations are consistent with previous work [9], and in the last section, we show that changes made to the main flame structure are the main driving mechanism in stabilising the system in the current configuration.

As expected, increasing L_c leads to a reduction of the oscillation frequency. This change is expected to be in the order $f \propto 1/L_c$ and is due to a change in the mode of the combustion chamber. There is also some variation in the frequency when V_H and $\bar{u}_1$ are varied, due to changes in the flame temperature and flame response. As the system approaches pure hydrogen $V_H = 1$ with $\bar{u}_1 = 30$ m/s, the oscillation frequency approaches values indicated by the dashed horizontal lines annotated $f_1 = 0.86$, $f_2 = 0.78$, and $f_3 = 0.64$ kHz. The impact of these in terms of changes in stability is discussed in Section 3.3 where the forced response is investigated.

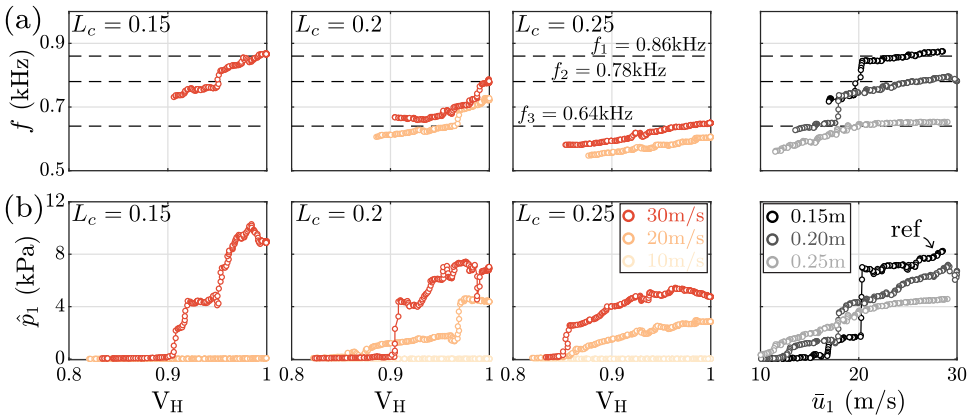

Fig. 4. Stability map when operating the main stage, i.e. with $\dot{V}_2 = 0$. (a) Fundamental mode frequency. (b) Pressure amplitude. Rows (1–3) show progressive increase of V_H, and row (4) show increase in $\bar{u}_1$.

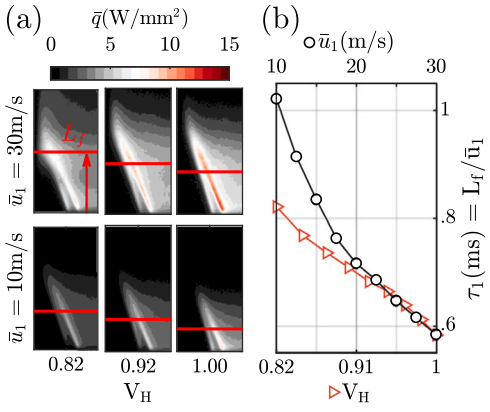

Fig. 5. (a) Mean flame images $\bar{q}$ shown for different V_H and $\bar{u}_1$. (b) Time delay τ_1 from Eq. (1).

3.2. Mitigation by staging and effect of interference

Having characterised regions of the operational map where instabilities occur, we now proceed to demonstrate a method to suppress them by distributing the flow between the two stages. For this purpose, the conditions summarised in the second and third row of Table 1 are discussed. Now, flow is introduced to the second stage, i.e. $\bar{u}_2$ is increased for either a fixed or reduced value of $\bar{u}_1$.

The resulting pressure amplitudes are displayed in Fig. 6 as a function of $\bar{u}_2$. In Fig. 6(a), the flow is divided between the two stages and the top axis indicates the corresponding reduction in the velocity provided to the first stage $\Delta\bar{u}_1$. The circular markers denote measurements taken over 30 s with fixed flow rates. At these points, high-speed imaging (shown in Fig. 8) of the flames were taken. The solid lines were obtained from linearly ramping the flow rates, in a similar way to the data presented in Fig. 3. These show reasonable agreement, which indicates that differences due to transients are not significant for the majority of operating points.

In Fig. 6(a), increasing $\bar{u}_2$ leads to a progressive reduction in the pressure amplitude for all conditions. For $L_c = 0.15$ m, the effect is significant, and it shows that by redistributing the flow to the second stage, a strong instability with an amplitude of ~ 9 kPa is completely suppressed. The effect is similar for the other lengths $L_c = 0.2$ and 0.25 m, although the reduction is less prominent. The reason for this variation with L_c is discussed in the last part of the paper.

The reduced amplitude observed in Fig. 6(a) may be driven by two main mechanisms. Firstly, reducing $\bar{u}_1$ increases τ_1 as shown in Fig. 4, which leads to a reduced excitation amplitude. Secondly, destructive interference may occur between the two flames Q_1 and Q_2. If the phase between these is such that they fully or partially cancel, the global fluctuation in HRR and thus the driving force will reduce. This effect on thermoacoustic systems has been investigated previously [8,36].

To decouple these two effects, $\bar{u}_2$ is varied while holding $\bar{u}_1$ constant. The pressure amplitude for these cases is shown in Fig. 6(b). Since $\bar{u}_1$ is kept fixed, the effect of reducing $\bar{u}_1$ is not present, and hence, the differences observed between cases shown in (a) and (b), are largely due to variations in $\bar{u}_1$. It is evident that an increase in $\bar{u}_2$ does not lead to the same reduction as observed in (a) for the majority of cases. As $\bar{u}_2$ increases in Fig. 6(b) the amplitudes remain similar for most cases, and for the case annotated 'B', the amplitude increases. An exception is observed for the case annotated }20 m/s', with $L_c = 0.15$, which becomes stable for $\bar{u}_2 > 35$ m/s, indicating that interference also plays a role.

The results shown Fig. 6(b) indicate that the main mechanism causing the reduced amplitude in (a), is linked to changes made to the flame structure when $\bar{u}_1$ is reduced. However, the effect of interference is still prominent and can act to augment the overall amplitude reduction. To show this, we focus on cases annotated A and B in Fig. 6. The pressure amplitude from these are plotted against $\bar{u}_1$ in Fig. 7, with the reference case, annotated 'ref' added as the black line. Again, it is important to note that for $\bar{u}_2 = 0$ both case A and B are at the same condition. However, when $\bar{u}_2$ is increased, this leads to a reduction in $\bar{u}_1$ for Case A, whereas for case B, the flow $\bar{u}_1$ is held fixed.

The amplitude of case A reduces significantly faster than for 'ref', as $\bar{u}_1$ is reduced, whereas the amplitude increases for case B. This suggests that interference contributes significantly to the pressure amplitude attenuation in case A. To understand why this occurs, the phase difference between Q_1, Q_2 is shown in Fig. 7(b) for cases A and B.

For case B where there is a progressive increase in the pressure amplitude, the global HRR of each of the two flames Q_1 and Q_2 oscillates in phase for all values of $\bar{u}_2$. As such, the second flame adds more driving force to the system, resulting in higher pressure amplitudes. Also, the fixed phase indicates that, despite the large increase in $\bar{u}_2$, the time delay of Q_2 remains unchanged.

For case A, where $\bar{u}_1$ is reduced whilst $\bar{u}_2$ is increased, the opposite occurs. At low values of $\bar{u}_2$, the two flames oscillate in phase, similar to case B. However, as $\bar{u}_2$ is increased and $\bar{u}_1$ is reduced, the phase difference between Q_1 and Q_2 increases progressively. At $\bar{u}_2 \approx 50$ m/s, the two flames oscillate in phase opposition which indicates destructive interference. In addition to the effect of reducing $\bar{u}_1$, the interference attenuates the global HRR fluctuations and hence, suppresses the driving term accordingly.

To show this effect visually, phase-averaged images of q_1 and q_2 are displayed in Fig. 8 at three phase angles $t/T = 0$, 0.25, and 0.5. The phase $t/T = 0.5$ corresponds to peak HRR of Q_1. Results are shown

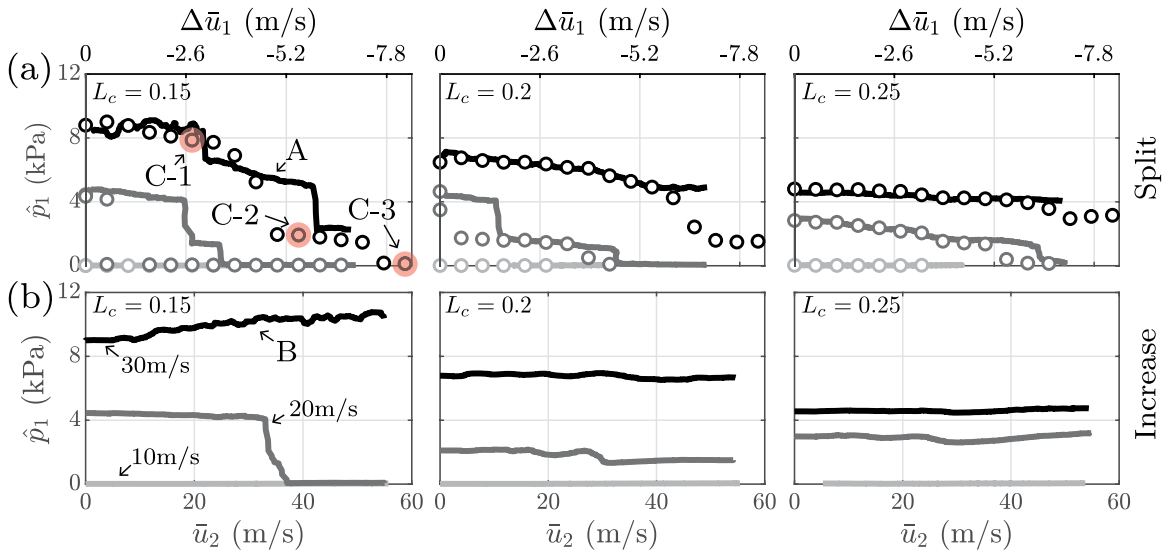

Fig. 6. Influence of the second stage flame on the pressure amplitude of the system. (a) Splitting the flow between the two stages. (b) Increasing the flow to stage 2 for a fixed value of $\bar{u}_2$. Markers in (a) indicate fixed measurements where C-1, C-2, and C-2 correspond to images in Fig. 8.

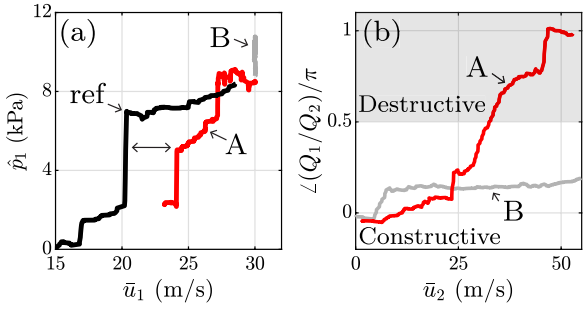

Fig. 7. Effect of interference between Q_1 and Q_2. (a) Pressure amplitude for cases annotated 'ref' in Fig. 4 and 'A' and 'B' in Fig. 6. (b) Phase difference between Q_1 and Q_2.

for the three cases annotated C-1, C-2, and C-3 in Fig. 6, where the system transitions from unstable to stable. The integrated HRR from the two flames Q_1 and Q_2 are displayed in Fig. 6(a). From top to bottom in Fig. 6(b), the images are shown at different phases $t/T = 0$, 0.25, and 0.5, with respect to the oscillation in the global HRR of Q_1, corresponding to markers in (a).

For C-1, the two flames oscillate in phase with large amplitude fluctuations (100% for Q_1 and 40% for Q_2). At $C-2$ the topology of the jet flame is more stabilised, due to the increased flow rate $\bar{u}_2$. The fluctuations of Q_1 and Q_2 have been significantly reduced compared to C-1, where Q_1 has relative fluctuations of about 40%. Furthermore, the two flames oscillate in phase opposition, as was shown in Fig. 7(b), which leads to a reduced global HRR fluctuation. At C-3, the system is stabilised with little to no fluctuations in Q_1 and Q_2.

3.3. Forced response

Although the effect of interference between the two flames is a contributing factor, the dominant mechanism causing stabilisation is a change in the main flame structure due to a reduction in $\bar{u}_1$. As already discussed, this leads to a change in τ_1, and here we show how this variation is consistent with a change in the flame response through measurements of the flame transfer function (FTF) of the main flame, i.e. with $\bar{u}_2 = 0$.

We follow the same procedure as [9] to measure FTFs. External acoustic forcing combined with the multiple microphone method were used to impose a fixed velocity perturbation amplitude of $|\hat{u}_1|/\bar{u}_1 = 0.05$ at the flame base for frequencies $f = 0.05 - 1.25$ kHz. The linear flame response is then quantified as the normalised fluctuations in $\hat{Q}_1$ divided by the acoustic velocity $\hat{u}_1$: $\mathrm{FTF}(f) = (\hat{Q}_1/\bar{Q}_1)/(\hat{u}_1/\bar{u}_1) = G\exp(\mathrm{j}\Theta)$, where G is the gain and Θ is the phase delay between the two signals. $\hat{u}_1$ is obtained using the multiple microphone method [37]. For low values of G, the flame is less effective at driving an instability at that frequency.

In Fig. 9(a), G and Θ are shown for $\mathrm{V_H} = 1$ with $\bar{u}_1 = 10$, 20, and 30 m/s. As discussed in [9], the FTFs of these flames behave as low-pass filters with an approximately linear phase slope $\Delta\Theta \approx -2\pi f\tau$, and a cut-off frequency $\omega_c \sim 1/\tau$. As was shown in Fig. 5, increasing $\bar{u}_1$ leads to a decrease in τ_1, and in Fig. 9(a) a corresponding increase in ω_c and decrease in the phase slope are observed as annotated by the red arrows. This is consistent with the trend observed in Fig. 4, where a reduction in $\bar{u}_1$ leads to stable operation.

The same effect occurs when $\mathrm{V_H}$ is varied for a fixed value of $\bar{u}_1$. This is shown in Fig. 9(b), where G is plotted at a fixed frequency $f = 0.8$ kHz, where $\bar{u}_1$ (panel 1) and $\mathrm{V_H}$ (panel 2) are varied over the same range as in Fig. 4. The top axis shows the corresponding values of τ_1. As either $\bar{u}_1$ or $\mathrm{V_H}$ are reduced, τ_1 increases, which leads to a reduction in the gain G. This shows that the effect of varying $\bar{u}_1$ and $\mathrm{V_H}$ are very similar in terms of the flame response.

To show that this change in the flame response is consistent with changes in the stability of the system, Fig. 9(c) shows data from Fig. 4 superimposed on a contour map of τ_1. The size and colour of the circular markers indicate the pressure amplitude $\hat{p}_2$, and the white crosses indicate stable operation. The panels annotated (1–3) show data for $L_c = 0.15$, 0.2, and 0.25 respectively. These cases correspond to different mode frequencies $f_1 = 0.86$, $f_2 = 0.78$, and $f_3 = 0.64$ kHz, obtained from Fig. 4. To link these to changes in the flame response, red solid lines indicate the normalised frequencies $f\tau_1 = 0.5$. For $f\tau_1 > 0.5$ the gain reduces, as shown in Fig. 9(b), where $f_{1-3}\tau_1 = 0.5$ are indicated by vertical lines.

As L_c is increased in Fig. 9(c), the region of $\bar{u}_1$ and $\mathrm{V_H}$ where the system is unstable expands towards lower values. This is consistent with a decrease in f that leads to a shift of the line $f\tau_1 = 0.5$ as annotated by the red arrows. For lower values of $f\tau_1$, G is progressively reduced and shows that the changes in stability are mainly due to a change in the flame structure that leads to a corresponding change in the flame response. Furthermore, these results show that the method is more effective at mitigating instabilities at high frequencies, as these

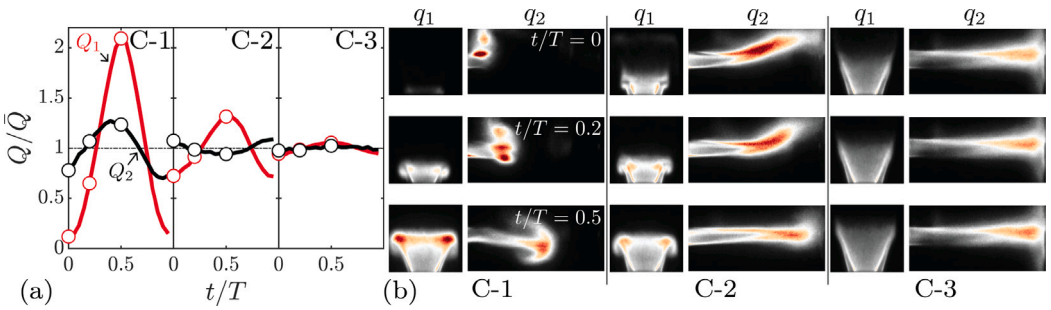

Fig. 8. Phase average images of q_1 and q_2 displayed for cases C-1, C-2, and C-3 in Fig. 6(a). (a) Global HRR Q_1 and Q_2. (b) Images at $t/T = 0$, 0.25, 0.5, corresponding to the circular markers in (a).

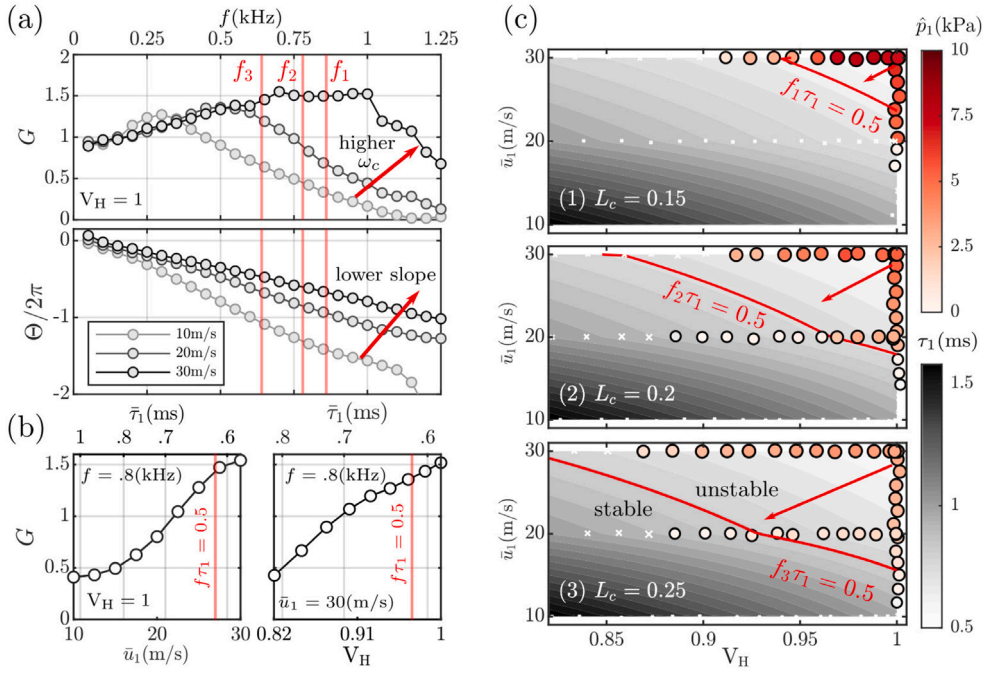

Fig. 9. (a-b) FTF measurements. (c) Pressure amplitude from Fig. 4 superimposed on contours of $\tau_1 = L_f/\bar{u}_1$. The red lines show $f\tau = 0.5$, where $f_{1,2,3} = 0.86, 0.78$ and 0.64 kHz from modes in Fig. 4.

are closer to the gain cut-off frequency of the first stage flame. It also explains why distributing the flow to the secondary flame is more effective for $L_c = 0.15$ compared to $L_c = 0.2$ and $L_c = 0.25$ in Fig. 6(a).

Ultimately, the stability map of a combustion system depends on the geometry and varies with operational parameters [7,13]. However, having a flexible sequential combustion system allows for distributing the flow in such a way that conditions that drive instabilities can potentially be avoided.

4. Conclusions

In this paper, we have demonstrated how axial staging can be used to mitigate thermoacoustic instabilities arising in combustion systems. Stability maps were measured when operating the system using the first stage, and high amplitude instabilities arise when increasing the hydrogen concentration or the total flow rate. This is consistent with other experimental observations of premixed hydrogen flames [7]. Flow was then introduced to the second stage, and we show that the system can be stabilised for most conditions, increasing the viable operational map significantly.

Two driving/damping effects were discussed and analysed in detail. The first and primary effect was shown to be that, as flow is reduced in the first stage flame, this leads to a change in the flame structure and thus, a reduced flame response to acoustic oscillations. Secondly, interference between the two flames was shown to play a role in suppressing the global fluctuation in the heat release rate. However, for the conditions considered in this paper, the former effect was shown to be the most significant, whereas the latter plays only a secondary role.

Novelty and significance statement

The novelty of this research is the demonstration of the beneficial effect of combustion staging on thermoacoustic stabilty. In particular, we demonstrate how high amplitude and frequency instabilities can be suppressed through flame distribution without modifying total flows or thermal power. As the authours have shown in previous work (15), this beneficial staging strategy can be used to greatly increase the achievable power density for pure hydrogen premixed flames without instability. A key strength of this work is that the experimental rig is an extension of a widely studied simple bluff-body-stabilised combustor (7, 8, 19), and a canonical jet-in-crossflow flame. This simplicity allows the use of well-established analysis to study why staging is effective in mitigating instability, while also demonstrating the importance of novel flame-flame interaction.

CRediT authorship contribution statement

Aksel Ånestad: Designed research, Performed experiments, Analysed data, Writing – original draft, Writing – review & editing. **Eirik Æsøy:** Designed research, Performed experiments, Analysed data, Writing – original draft, Writing – review & editing. **James R. Dawson:** Designed research, Reviewed the paper. **Nicholas A. Worth:** Designed research, Writing – review & editing.

Declaration of competing interest

The authors declare that they have no known competing financial interests or personal relationships that could have appeared to influence the work reported in this paper.

Acknowledgements

The authors acknowledge funding from the LowEmission Research Centre, performed under the Norwegian research program PETROSENTER, and the Research Council of Norway (Grant number 296207).

References

[1] M.R. Bothien, A. Ciani, J.P. Wood, G. Fruechtel, Toward decarbonized power generation with gas turbines by using sequential combustion for burning hydrogen, J. Eng. Gas Turbines Power 141 (12) (2019) 121013.
[2] J. Beita, M. Talibi, S. Sadasivuni, R. Balachandran, Thermoacoustic instability considerations for high hydrogen combustion in lean premixed gas turbine combustors: a review, Hydrogen 2 (1) (2021) 33–57.
[3] H. Kobayashi, A. Hayakawa, K.K.A. Somarathne, E.C. Okafor, Science and technology of ammonia combustion, Proc. Combust. Inst. 37 (1) (2019) 109–133.
[4] E.C. Okafor, K.K.A. Somarathne, A. Hayakawa, T. Kudo, O. Kurata, N. Iki, H. Kobayashi, Towards the development of an efficient low-NOx ammonia combustor for a micro gas turbine, Proc. Combust. Inst. 37 (4) (2019) 4597–4606.
[5] M.-C. Chiong, C.T. Chong, J.-H. Ng, S. Mashruk, W.W.F. Chong, N.A. Samiran, G.R. Mong, A. Valera-Medina, Advancements of combustion technologies in the ammonia-fuelled engines, Energy Convers. Manag. 244 (2021) 114460.
[6] T.C. Lieuwen, V. Yang, Combustion Instabilities in Gas Turbine Engines: Operational Experience, Fundamental Mechanisms, and Modeling, AIAA, 2005.
[7] J.G. Aguilar, E. Æsøy, J.R. Dawson, The influence of hydrogen on the stability of a perfectly premixed combustor, Combust. Flame 245 (2022) 112323.
[8] E. Æsøy, T. Indlekofer, F. Gant, A. Cuquel, M.R. Bothien, J.R. Dawson, The effect of hydrogen enrichment, flame-flame interaction, confinement, and asymmetry on the acoustic response of a model can combustor, Combust. Flame 242 (2022) 112176.
[9] E. Æsøy, J.G. Aguilar, S. Wiseman, M.R. Bothien, N.A. Worth, J.R. Dawson, Scaling and prediction of transfer functions in lean premixed H2/CH4-Flames, Combust. Flame 215 (2020) 269–282.
[10] H. Kang, K.T. Kim, Combustion dynamics of multi-element lean-premixed hydrogen-air flame ensemble, Combust. Flame 233 (2021) 111585.
[11] H. Kang, M. Lee, K.T. Kim, Measurements of self-excited instabilities and nitrogen oxides emissions in a multi-element lean-premixed hydrogen/methane/air flame ensemble, Proc. Combust. Inst. 39 (4) (2023) 4721–4729.
[12] T. Lee, K.T. Kim, Combustion dynamics of lean fully-premixed hydrogen-air flames in a mesoscale multinozzle array, Combust. Flame 218 (2020) 234–246.
[13] Y. Choi, K.T. Kim, Mode shape-dependent thermoacoustic interactions between a lean-premixed primary flame and an axially-staged transverse reacting jet, Combust. Flame 255 (2023) 112884.
[14] J. McClure, M. Bothien, T. Sattelmayer, High-frequency mode shape dependent flame-acoustic interactions in reheat flames, J. Eng. Gas Turbines Power 145 (1) (2023) 011014.
[15] A. Ånestad, R. Sampath, J. Moeck, A. Gruber, N. Worth, The structure and stability of premixed CH4, H2, and NH3/H2 flames in an axially staged can combustor, J. Eng. Gas Turbines Power (2023) 1–13.
[16] T. Poinsot, Prediction and control of combustion instabilities in real engines, Proc. Combust. Inst. 36 (1) (2017) 1–28.
[17] J. O'Connor, Understanding the role of flow dynamics in thermoacoustic combustion instability, Proc. Combust. Inst. 39 (4) (2023) 4583–4610.
[18] T. Lee, K.T. Kim, High-frequency transverse combustion instabilities of lean-premixed multislit hydrogen-air flames, Combust. Flame 238 (2022) 111899.
[19] E. Æsøy, H.T. Nygård, N.A. Worth, J.R. Dawson, Tailoring the gain and phase of the flame transfer function through targeted convective-acoustic interference, Combust. Flame 236 (2022) 111813.
[20] E. Æsøy, The Effect of Hydrogen Enrichment on the Thermoacoustic Behaviour of Lean Premixed Flames (Ph.D. thesis), NTNU, 2022.
[21] D. Noble, D. Wu, B. Emerson, S. Sheppard, T. Lieuwen, L. Angello, Assessment of current capabilities and near-term availability of hydrogen-fired gas turbines considering a low-carbon future, J. Eng. Gas Turbines Power 143 (4) (2021).
[22] J.M. Beér, Combustion technology developments in power generation in response to environmental challenges, PECS 26 (4–6) (2000) 301–327.
[23] J. McClure, M. Bothien, T. Sattelmayer, Autoignition delay modulation by high-frequency thermoacoustic oscillations in reheat flames, Proc. Combust. Inst. 39 (4) (2023) 4691–4700.
[24] O. Schulz, U. Doll, D. Ebi, J. Droujko, C. Bourquard, N. Noiray, Thermoacoustic instability in a sequential combustor: Large eddy simulation and experiments, Proc. Combust. Inst. 37 (4) (2019) 5325–5332.
[25] Y. Xiong, J. Droujko, O. Schulz, N. Noiray, Investigation of thermoacoustic instability in sequential combustor during first stage lean blow-off, Proc. Combust. Inst. 38 (4) (2021) 6165–6172.
[26] B. Dharmaputra, S. Shcherbanev, B. Schuermans, N. Noiray, Thermoacoustic stabilization of a sequential combustor with ultra-low-power nanosecond repetitively pulsed discharges, Combust. Flame 258 (2023) 113101.
[27] D.A. Pennell, M.R. Bothien, A. Ciani, V. Granet, G. Singla, S. Thorpe, A. Wickstroem, K. Oumejjoud, M. Yaquinto, An introduction to the Ansaldo GT36 constant pressure sequential combustor, in: Turbo Expo: Power for Land, Sea, and Air, Volume 4B: Combustion, Fuels and Emissions, 2017, V04BT04A043.
[28] O. Schulz, N. Noiray, Autoignition flame dynamics in sequential combustors, Combust. Flame 192 (2018) 86–100.
[29] E. Æsøy, G.K. Jankee, S. Yadala, N.A. Worth, J.R. Dawson, Suppression of self-excited thermoacoustic instabilities by convective-acoustic interference, Proc. Combust. Inst. 39 (4) (2023) 4611–4620.
[30] J.A. Wagner, S.W. Grib, M.W. Renfro, B.M. Cetegen, Flowfield measurements and flame stabilization of a premixed reacting jet in vitiated crossflow, Combust. Flame 162 (10) (2015) 3711–3727.
[31] J.A. Wagner, S.W. Grib, J.W. Dayton, M.W. Renfro, B.M. Cetegen, Flame stabilization analysis of a premixed reacting jet in vitiated crossflow, Proc. Combust. Inst. 36 (3) (2017) 3763–3771.
[32] M.D. Pinchak, V.G. Shaw, E.J. Gutmark, The effects of nozzle geometry and equivalence ratio on a premixed reacting jet in vitiated cross-flow, Combust. Flame 191 (2018) 353–367.
[33] B. Higgins, M. McQuay, F. Lacas, J.-C. Rolon, N. Darabiha, S. Candel, Systematic measurements of OH chemiluminescence for fuel-lean, high-pressure, premixed, laminar flames, Fuel 80 (1) (2001) 67–74.
[34] E. Æsøy, J.R. Dawson, J.P. Moeck, Systematic modulation of the flame transfer function and its effect on thermoacoustic stability, Combust. Flame 265 (2024) 113494.
[35] T. Indlekofer, A. Faure-Beaulieu, N. Noiray, J. Dawson, The effect of dynamic operating conditions on the thermoacoustic response of hydrogen rich flames in an annular combustor, Combust. Flame 223 (2021) 284–294.
[36] N. Noiray, D. Durox, T. Schuller, S. Candel, Dynamic phase converter for passive control of combustion instabilities, Proc. Combust. Inst. 32 (2) (2009) 3163–3170.
[37] A.F. Seybert, D.F. Ross, Experimental determination of acoustic properties using a two-microphone random-excitation technique, J. Acoust. Soc. 61 (5) (1977) 1362–1370.